

IGNITION ENERGY SCALING OF INERTIAL CONFINEMENT FUSION TARGETS

M.M. BASKO*, J. JOHNER
DRFC, CEA Cadarache,
St. Paul-lez-Durance,
France

ABSTRACT. Scaling of the ignition energy threshold E_{ig} with the implosion velocity v_{im} and isentrope parameter α of imploding spherical DT shells is investigated by performing one dimensional (1-D) hydrodynamic simulations of the implosion and hot spot formation dynamics. It is found that the a and b exponents in the power law approximation $E_{\text{ig}} \propto \alpha^a v_{\text{im}}^{-b}$ depend crucially on the subset of initial configurations chosen to establish the scaling law. When the initial states are generated in the same way as in the Livermore study (W.K. Levedahl, J.D. Lindl, Nucl. Fusion **37** (1997) 165), the same scaling, $E_{\text{ig}} \propto \alpha^{1.7} v_{\text{im}}^{-5.5}$, is recovered. If, however, the initial states are generated by rescaling the parent configuration according to the hydrodynamic similarity laws, a different scaling is obtained, $E_{\text{ig}} \propto \alpha^{3.0} v_{\text{im}}^{-9.1}$, which is very close to the $\alpha^3 v_{\text{im}}^{-10}$ dependence predicted by the simple isobaric model for assembled fuel states. The latter is more favourable than the Livermore scaling when rescaling the fusion capsules to higher implosion velocities, but requires the peak drive pressure to be increased as $P \propto v_{\text{im}}^5$.

1. INTRODUCTION

The physical scale and the costs of an ICF ignition facility depend crucially on the minimum energy required to drive a fusion pellet to ignition. In the classical scheme of ignition, initiated at a central hot spot surrounded by a spherical shell of low entropy fuel, the dependence of the ignition threshold E_{ig} on the implosion velocity v_{im} and the entropy (compressibility) parameter α of the cold fuel plays a central role for defining the driver requirements and the implosion strategy. For about a decade the Livermore group has been quoting a power law scaling of

$$E_{\text{ig}} \propto \alpha^a v_{\text{im}}^{-b} \quad (1)$$

[1–4] with somewhat differing values of the exponents a and b . In their latest and most detailed publication on the subject [4], the values $a = 1.7 \pm 0.2$ and $b = 5.5 \pm 0.5$ have been given.

The Livermore scaling was obtained by fitting the results of a series of LASNEX simulations performed for a certain subset of imploding fuel configurations [4]. At the same time, several attempts have been undertaken to derive this scaling analytically (or semi-analytically) by analysing the fuel states near the time of maximum compression. The simplest static isobaric model for assembled DT configurations [5, 6] predicts a scaling, $E_{\text{ig}} \propto \alpha^3 v_{\text{im}}^{-10}$, which differs

significantly from that of Ref. [4]. In Ref. [7] it was shown that the dynamic effect of a scale dependent time of inertial confinement, in combination with a more realistic pressure profile, reduces the value of the exponent b from 10 to 7. Piriz [8] applied analytical methods to treat the dynamics of ignition profile formation under the influence of heat conduction and α particle transport and obtained $E_{\text{ig}} \propto v_{\text{im}}^{-5}$. His result seemed to corroborate the conclusion of Ref. [4] that it is these latter processes which stipulate the departure of the Livermore scaling from the $\alpha^3 v_{\text{im}}^{-10}$ law.

In this article, we investigate the scaling of E_{ig} with α and v_{im} by performing numerical simulations of imploding DT shells with the one dimensional (1-D) three temperature (3-T) DEIRA code [9]. We employ the same method as in Ref. [4] and, having assigned the same initial conditions, reproduce the Livermore scaling. As the next step, we establish an alternative scaling law, $E_{\text{ig}} \propto \alpha^{3.0} v_{\text{im}}^{-9.1}$, which includes the same physics of the hot spot formation but is based on a different subset of initial configurations. The latter is obtained by rescaling the parent configuration according to the laws of hydrodynamic similarity and appears to be no less relevant to ICF studies than the one used in Ref. [4]. We conclude that the departure of the Livermore scaling from the one derived in the isobaric model is caused mainly by the specific procedure used to generate the specific subset of initial states. The final judgement on the applicability of a particular scaling law should be

* *On leave from:* The Institute for Theoretical and Experimental Physics, Moscow, Russian Federation.

made on the basis of particular constraints pertaining to the relevant drive conditions.

2. LIVERMORE SCALING REPRODUCED

The Livermore scaling law for E_{ig} has been obtained from a series of numerical simulations with the LASNEX code [4]. Although LASNEX is a 2-D code, the scaling in question has apparently been derived within purely 1-D physics. Since we employ a different 1-D code for the present study, our first task will be to verify the Livermore scaling under similar initial conditions.

2.1. Method

The method employed in Ref. [4] consists of two principal steps. First, a suitable initial configuration of the imploding DT fuel at maximum implosion velocity is isolated from an efficiently performing X ray driven fusion capsule. Then, a specific three parameter rescaling procedure is applied to this parent configuration to generate a 3-D continuum of the initial states for subsequent LASNEX runs. One of the three parametric dimensions (mass rescaling) is used to find the ignition threshold E_{ig} , and the other two (velocity and entropy rescalings) allow the dependence $E_{\text{ig}}(\alpha, v_{\text{im}})$ to be calculated. We apply this same method throughout our study and do not check whether the scaling laws thus obtained are reproduced in full target simulations starting at the onset of laser (or particle) irradiation.

2.2. Parent configuration

The parent configuration used in Ref. [4] has been obtained by optimizing the performance of an X ray driven fusion capsule composed of a 0.87 mg solid DT shell surrounded by an LiD ablator. The initial state for the scaling study is taken for the imploding DT shell in flight, when the ablator material has been practically fully evaporated and the shell has reached its maximum velocity. This corresponds approximately to the moment when the first shock has just converged upon the centre, and the dense DT shell is at about a quarter of its initial radius.

Because the parent configuration of Ref. [4] cannot be reproduced literally without access to the authors' numerical data, we approximate it with the idealized in-flight DT configuration shown in Fig. 1. The imploding fuel consists of two regions: the central gas region, $0 \leq r < R_{\text{h}}$, is surrounded by a low

entropy dense shell, $R_{\text{h}} < r < R_0$. The initial state is described analytically and is fully determined by the values of the following six independent parameters:

$$M, R_0, v_{\text{im}}, \alpha, \xi_{\text{h}}, \mu_{\text{h}}. \quad (2)$$

Here M is the total fuel mass, R_0 is its initial outer radius, v_{im} is the implosion velocity, α is the entropy (compressibility) parameter of the cold fuel defined by Eqs (4) and (5) below, $\xi_{\text{h}} = R_{\text{h}}/R_0$ is the initial fractional radius of the hot spot and $\mu_{\text{h}} = M_{\text{h}}/M$ is the initial fraction of the fuel mass in the hot spot. In terms of the fractional radius, $\xi = r/R_0$, the initial density and pressure profiles are taken in the form

$$\rho(\xi) = \begin{cases} \rho_{\text{h}0}, & 0 \leq \xi \leq \xi_{\text{h}} \\ \rho_0 \left(\frac{\xi - \xi_*}{1 - \xi_*} \right)^{3/2}, & \xi_* < \xi_{\text{h}} < \xi \leq 1 \end{cases} \quad (3)$$

$$P(\xi) = \begin{cases} P_{\text{h}0}, & 0 \leq \xi \leq \xi_{\text{h}} \\ P_* \alpha [\rho(\xi)]^{5/3}, & \xi_* < \xi_{\text{h}} < \xi \leq 1 \end{cases} \quad (4)$$

where

$$P_* = \frac{(3\pi^2)^{2/3} \hbar^2}{5m_e (Am_A)^{5/3}} = 2.18 \text{ Mbar} \cdot \text{cm}^5 \cdot \text{g}^{-5/3} \quad (5)$$

for the equimolar DT mixture with $A = 2.5$, and α , $\rho_{\text{h}0}$, ρ_0 , ξ_* and $P_{\text{h}0}$ are constants. Following Ref. [4], we start at the time when the first shock has just reached the target centre and assign a constant initial value, $v(\xi) = -v_{\text{im}}$, of the radial velocity v to all the fluid elements.

The profiles (3) and (4) in the cold shell correspond to an idealized situation when the fluid elements, obeying the barotropic law $P \propto \rho^{5/3}$, all have one and the same radial acceleration, $g = -\rho^{-1} (\partial P / \partial r)$. Because we assume zero boundary pressure for all subsequent times, this idealization corresponds to instantaneous unloading of the outer fuel boundary at $t = 0$, and, as a consequence, results in somewhat unrealistic initial density and pressure peaks at the outer fuel edge $r = R_0$ (Fig. 1), which exceed considerably the corresponding peak values of the Livermore initial state [4]. This fact, however, has little influence on the ignition energy scaling because, for one reason, our sharp initial pressure (density) peak is quickly smeared by subsequent hydrodynamic evolution and approaches that of Ref. [4]. Also, the ignition threshold appears to be sensitive to the inner density profile in the vicinity of the cold-hot fuel interface, which is expected to be adequately reproduced by Eqs (3) and (4), but not to the initial peak at the fuel periphery. Exact initial profiles in the hot gas

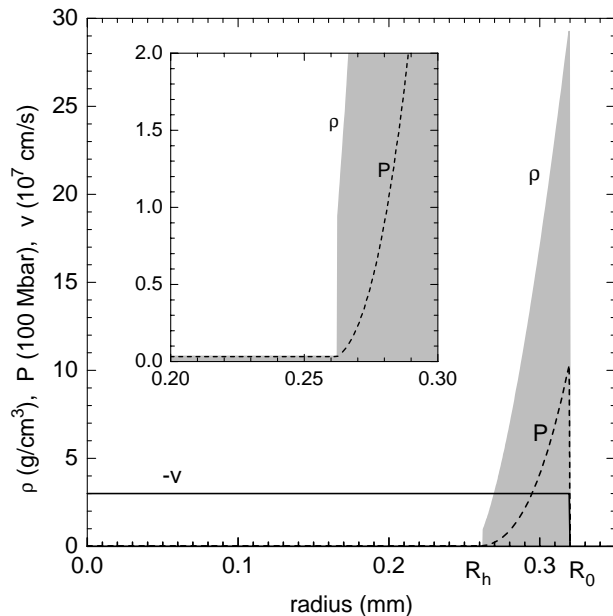


FIG. 1. Initial state of the imploding DT fuel used as a parent configuration for the scaling study. It is an analytical approximation, as given by Eqs (3) and (4), to the initial state of Ref. [4] with $\alpha = 1.7$.

region are also of little importance because of a rapid subsequent self-regulatory relaxation due to the electron heat conduction and radiation transport. Hence, we adopt the simplest uniform initial structure of the hot spot at $0 \leq \xi \leq \xi_h$.

Since the shock fronts of the drive phase have already passed through the hot-cold fuel interface, we assume that the pressure is continuous at $\xi = \xi_h$, i.e.

$$P_{h0} = P_* \alpha \rho_0^{5/3} \left(\frac{\xi_h - \xi_*}{1 - \xi_*} \right)^{5/2} \quad (6)$$

but admit a density (hence an entropy) jump across this interface. The constant ξ_* can be expressed in terms of the basic parameters (2) by invoking the following consideration. The energy which resides in the imploding fuel, and which is predominantly the kinetic energy split in the ratio $M_h:M$ between the hot and total fuel, has been supplied by the $P dV$ work during the drive phase. Hence, the ratio of the drive pressure values between the inner and the outer edges of the thin cold shell can be approximated as

$$\frac{P_{h0}}{P_* \alpha \rho_0^{5/3}} = \frac{M_h}{M} \equiv \mu_h. \quad (7)$$

From Eqs (6) and (7) we calculate

$$\xi_* = \frac{\xi_h - \mu_h^{2/5}}{1 - \mu_h^{2/5}}. \quad (8)$$

The density values ρ_{h0} and ρ_0 are calculated from the conditions of mass balance for the hot and cold fuel regions:

$$\rho_{h0} = \frac{3}{4\pi} \frac{\mu_h M}{R_0^3 \xi_h^3} \quad (9)$$

$$\rho_0 = \frac{1}{4\pi R_0^3} \left(\frac{1 - \xi_h}{1 - \mu_h^{2/5}} \right)^{3/2} \frac{(1 - \mu_h)M}{\Phi_M(1, \xi_*) - \Phi_M(\xi_h, \xi_*)} \quad (10)$$

where

$$\begin{aligned} \Phi_M(\xi, \xi_*) &= \int_{\xi_*}^{\xi} (x - \xi_*)^{3/2} x^2 dx \\ &= \frac{2}{9} (\xi - \xi_*)^{9/2} + \frac{4}{7} \xi_* (\xi - \xi_*)^{7/2} + \frac{2}{5} \xi_*^2 (\xi - \xi_*)^{5/2}. \end{aligned} \quad (11)$$

Trying to reproduce as closely as possible the parent configuration of Ref. [4], we have chosen for the simulations discussed below the following set of basic parameter values:

$$M = 0.87 \text{ mg}, \quad R_0 = 0.32 \text{ mm}, \quad v_{\text{im}} = 3 \times 10^7 \text{ cm/s}$$

$$\alpha = 1.7, \quad \xi_h = 0.82, \quad \mu_h = 0.003.$$

The above value of μ_h assumes that the initial mass of the DT gas fill is preserved until the maximum implosion velocity is reached. According to Levedahl and Lindl [4], their parent configuration ignites at $v_{\text{im}} \approx 2.35 \times 10^7 \text{ cm/s}$. We obtain ignition (as defined in Section 2.4 below) at $v_{\text{im}} = 2.51 \times 10^7 \text{ cm/s}$, which, in view of all the differences between the codes and the initial states, can be considered as a good agreement.

2.3. Rescaling procedure

In terms of our six basic parameters (2), the rescaling procedure of the parent configuration adopted in Ref. [4] is as follows:

(a) Mass rescaling,

$$R_0 \rightarrow R'_0 = X \cdot R_0, \quad M \rightarrow M' = X^3 M \quad (12)$$

$$v_{\text{im}}, \alpha, \xi_h, \mu_h = \text{invariant}$$

(b) Velocity rescaling,

$$v_{\text{im}} \rightarrow v'_{\text{im}} = Y \cdot v_{\text{im}} \quad (13)$$

$$M, R_0, \alpha, \xi_h, \mu_h = \text{invariant}$$

(c) Entropy rescaling,

$$\alpha \rightarrow \alpha' = Z \cdot \alpha, \quad \xi_h \rightarrow \xi'_h, \quad R_0 \rightarrow R'_0 = \frac{\xi_h}{\xi'_h} R_0 \quad (14)$$

$M, v_{\text{im}}, \mu_h = \text{invariant.}$

The value of ξ'_h as a function of ξ_h, μ_h and the scaling factor Z is calculated from the equation

$$Z = \left(\frac{\xi_h^2(1 - \xi_h)}{\xi_h'^2(1 - \xi_h')} \right)^{5/2} \left(\frac{\Phi_M(1, \xi'_*) - \Phi_M(\xi'_h, \xi'_*)}{\Phi_M(1, \xi_*) - \Phi_M(\xi_h, \xi_*)} \right)^{5/3} \quad (15)$$

where $\xi'_* = (\xi'_h - \mu_h^{2/5}) / (1 - \mu_h^{2/5})$.

Here, only the entropy rescaling of the parameter α is non-trivial. It is done in such a way as to preserve the initial radius, $R_h = \xi_h R_0$, of the hot spot, and the initial pressure profile in the cold shell as a function of its mass co-ordinate. Equation (15) follows from the condition that the product $\alpha \rho_0^{5/3}$, which represents the peak pressure at the outer fuel edge, should remain invariant under the transformation (14). An important feature of this rescaling algorithm is that each transformation preserves the value of the pressure peak in the initial state of the fuel shell.

2.4. Simulation results

The initial fuel configurations described above were substituted into the 1-D, 3-T hydrodynamics code DEIRA [9], and their subsequent implosion and burn performance was calculated numerically. The DEIRA code includes the main physical processes which govern the spark ignition mode in DT, i.e. the electron heat conduction (flux limited), the energy transport by radiation (in the flux limited diffusion approximation for the radiation energy density aT_r^4) and the non-local energy deposition by α particles (in the diffusion approximation for the energy density of α particles). Non-local heating by thermonuclear DT and DD neutrons is also taken into account. The effects of electron degeneracy are fully accounted for in the equation of state, and when calculating the coefficients of the electron heat conduction and the mean Rosseland and Planckian opacities of the DT plasma. The ideal gas equation of state is used for the Boltzmann ions and Fermi electrons. The Fermi integrals are approximated by simple analytical formulas, as described in Ref. [10].

For each combination of the X, Y, Z scaling factors, a DEIRA run was performed and the value of the

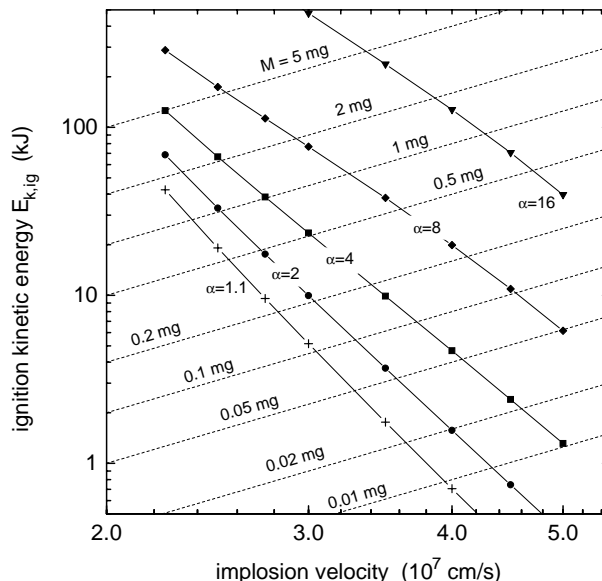


FIG. 2. Initial kinetic energy of imploding fuel for marginally igniting configurations ($G_f = 8$) as a function of the implosion velocity v_{im} for five different values of the entropy parameter α . The initial states are generated by applying the Livermore rescaling procedure.

fuel energy gain G_f (defined as the ratio of the thermonuclear yield to the total initial fuel energy) was calculated. By varying the value of X , an ignition threshold was found for each Y, Z pair. The ignition threshold is defined as the value $G_f = 8$, which would correspond to the ‘breakeven’ condition for fusion capsules with a fixed 12.5% hydrodynamic efficiency of the ablative acceleration. Here, following Ref. [4], we consider the dependence of the initial kinetic energy $E_{k,\text{ig}} = \frac{1}{2} M_{\text{ig}} v_{\text{im}}^2$ at the ignition threshold on parameters Y, Z , i.e. on v_{im} and α . Note that $E_{k,\text{ig}}$ is only a part, though a dominant one, of the total initial fuel energy E_{ig} . The relation to the scaling of the total ignition energy E_{ig} is discussed in Section 4.3.

Figure 2 shows the calculated dependence $E_{k,\text{ig}}(\alpha, v_{\text{im}})$ in a double logarithmic scale. Clearly, it can be approximated with a power law, although the accuracy of such an approximation cannot be expected to be high. The values of the exponents a and b in Eq. (1), which give the best fit to the data presented in Fig. 2, are indeed very close to those ($a = 1.7, b = 5.5$) obtained in Ref. [4]. If we normalize the calculated values of $E_{k,\text{ig}}$ to the power law function $1.2 \text{ (kJ)} \alpha^{1.7} (v_{\text{im}} / 3.5 \times 10^7 \text{ cm/s})^{-5.5}$, we obtain the plot shown in Fig. 3. The ideal scaling would correspond to all the calculated points collapsed onto a single horizontal line. In the parameter range

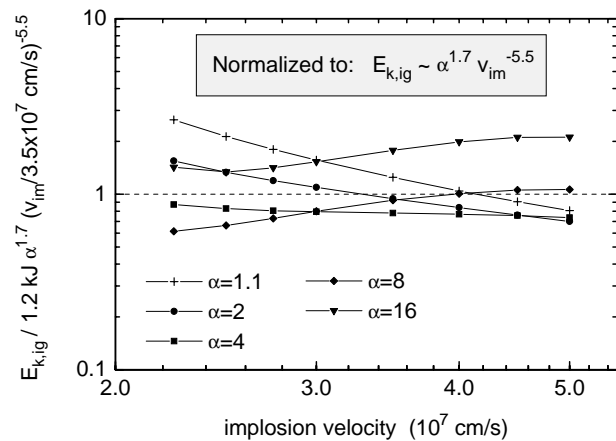


FIG. 3. Livermore scaling: same data as in Fig. 2 but normalized to the power law dependence $1.2 \text{ (kJ)} \alpha^{1.7} (v_{\text{im}}/3.5 \times 10^7 \text{ cm/s})^{-5.5}$.

considered, $1 < \alpha \leq 16$, $2.25 \times 10^7 \text{ cm/s} \leq v_{\text{im}} \leq 5 \times 10^7 \text{ cm/s}$, maximum deviations from this ideal scaling law amount to about a factor of 2. When we plot $E_{k,\text{ig}}(\alpha)$ for a fixed value of $v_{\text{im}} = 3.5 \times 10^7 \text{ cm/s}$, we obtain a curve which is hardly distinguishable from the analogous curve in Fig. 5 of Ref. [4].

Thus, our numerical simulations do reproduce the Livermore scaling of the ignition energy when an analogous parent configuration is chosen and the same three parameter rescaling procedure is applied. This gives us confidence that the main physical processes which determine the dependence $E_{k,\text{ig}}(\alpha, v_{\text{im}})$ calculated with the LASNEX code are also adequately described by the DEIRA code.

3. SCALING LAW FOR SELF-SIMILAR RESCALING OF THE INITIAL STATE

3.1. Self-similar rescaling procedure

As the next step, we take a closer look at the rescaling procedure described in Section 2.3. First of all, we note that the velocity and entropy rescalings violate the similarity of pure hydrodynamic motion. Indeed, the equations of the ideal (dissipationless) hydrodynamics for a fluid with the adiabatic index $\gamma = 5/3$,

$$\frac{\partial \rho}{\partial t} + \frac{1}{r^2} \frac{\partial}{\partial r} (r^2 \rho v) = 0 \quad (16)$$

$$\rho \frac{\partial v}{\partial t} + \rho v \frac{\partial v}{\partial r} + \frac{\partial P}{\partial r} = 0 \quad (17)$$

$$\frac{\partial}{\partial t} \left(\frac{3P}{2\rho} \right) + v \frac{\partial}{\partial r} \left(\frac{3P}{2\rho} \right) + \frac{P}{\rho} \frac{1}{r^2} \frac{\partial}{\partial r} (r^2 v) = 0 \quad (18)$$

remain invariant with respect to the following three rescaling transformations:

(a) Mass rescaling,

$$t \rightarrow X \cdot t, \quad r \rightarrow X \cdot r, \quad m \rightarrow X^3 m \quad (19)$$

$$v, \rho, P, \alpha \propto P/\rho^{5/3} = \text{invariant}$$

(b) Velocity rescaling,

$$t \rightarrow t/Y^2, \quad r \rightarrow r/Y, \quad v \rightarrow Y \cdot v$$

$$\rho \rightarrow Y^3 \rho, \quad P \rightarrow Y^5 P \quad (20)$$

$$m, \alpha = \text{invariant}$$

(c) Entropy rescaling,

$$t \rightarrow Z^{1/2} t, \quad r \rightarrow Z^{1/2} r, \quad \rho \rightarrow Z^{-3/2} \rho$$

$$P \rightarrow Z^{-3/2} P, \quad \alpha \propto P/\rho^{5/3} \rightarrow Z \cdot \alpha \quad (21)$$

$$v, m = \text{invariant.}$$

Here $m = 4\pi \int \rho r^2 dr$ is the mass between any two Lagrangian interfaces. In contrast to Eqs (13) and (14), the transformations (20) and (21) require rescaling of the radii, densities and pressures in all the fluid elements.

Clearly, if the implosion dynamics of the DT fuel were governed solely by Eqs (16)–(18) and, in addition, the initial state were rescaled according to the similarity laws (19)–(21), all the implosions from our 3-D X, Y, Z continuum of the implosion histories would evolve along similar sequences of hydrodynamic states. In other words, the 4-D t, X, Y, Z continuum of the fluid states would be self-similar along the X, Y, Z axes. Hence, we call the corresponding rescaling procedure a self-similar one. In particular, all the implosions would be characterized by the same aspect and radial convergence ratios, and, as a consequence, would have equivalent conditions for the development of the Rayleigh–Taylor instability.

In terms of the basic parameters (2), the self-similar rescaling of the parent configuration is given by

(a) Mass rescaling,

$$R_0 \rightarrow X \cdot R_0, \quad M \rightarrow X^3 M \quad (22)$$

$$v_{\text{im}}, \alpha, \xi_{\text{h}}, \mu_{\text{h}} = \text{invariant}$$

(b) Velocity rescaling,

$$v_{\text{im}} \rightarrow Y \cdot v_{\text{im}}, \quad R_0 \rightarrow R_0/Y \quad (23)$$

$$M, \alpha, \xi_h, \mu_h = \text{invariant}$$

(c) Entropy rescaling,

$$\alpha \rightarrow Z \cdot \alpha, \quad R_0 \rightarrow Z^{1/2} R_0 \quad (24)$$

$$M, v_{\text{im}}, \xi_h, \mu_h = \text{invariant.}$$

Equations (23) and (24) imply that, as contrasted to the Livermore rescaling procedure, the peak drive pressure in the fuel shell scales as $P \propto \alpha^{-3/2} v_{\text{im}}^5$.

One can point out at least two reasons why the self-similar rescaling of the parent configuration might be preferred (or, at least, should be considered on an equal basis) to that adopted in the Livermore study. The first is related to the hydrodynamic instability during the implosion stage. The most efficiently performing fusion capsules with different values of α and v_{im} should be able to tolerate approximately the same instability growth factors during the acceleration phase. This is ensured when implosions proceed along similar hydrodynamic states and, in particular, are characterized by the same in-flight aspect ratios when the main acceleration occurs [3]. Also, the scaling of the peak drive pressure with the implosion velocity, $P \propto T_r^{3.5} \propto v_{\text{im}}^{35/9}$, which one recovers from Eqs (51) and (62) of Ref. [3] (here T_r is the temperature of the thermal X rays which drive the implosion), is much closer to the hydrodynamic similarity scaling $P \propto v_{\text{im}}^5$ than to the fixed pressure assumed in Eq. (13).

The second reason is related to optimization of the fuel configurations at ignition. To illustrate the point, assume for the moment that the parent configuration has been optimized to produce the best ignition profiles in the fuel core at stagnation. However, once this initial configuration is rescaled to other values of α and v_{im} without reoptimization, the resulting ignition profiles would generally deviate from the optimal ones, and this deviation would generally have a different scale dependence for different rescaling procedures. One of the conclusions of our present study is that the self-similar rescaling of the initial state leads to better quality ignition profiles than the rescaling adopted in the Livermore study.

3.2. Ignition energy scaling

Having repeated the series of DEIRA simulations described in Section 2.4 with the self-similar rescaling

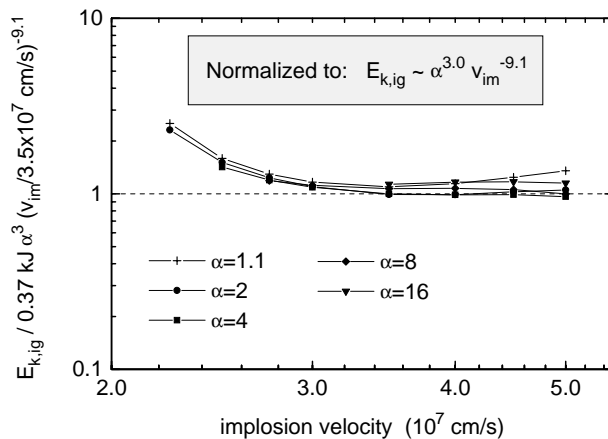


FIG. 4. HSI scaling: initial kinetic energy of marginally igniting configurations calculated with the self-similar rescaling of the initial state and normalized to the power law $0.37 \text{ (kJ)} \alpha^{3.0} (v_{\text{im}}/3.5 \times 10^7 \text{ cm/s})^{-9.1}$.

of the parent state, we found a significantly different scaling for the ignition energy E_{ig} , which corresponds to the values of $a = 3.0 \pm 0.1$ and $b = 9.1 \pm 0.2$ in Eq. (1). In these simulations we used exactly the same parent configuration as the one chosen in Section 2.2 to verify the Livermore scaling. Note that now, in contrast to the Livermore scaling, the initial kinetic energy, $E_{k,\text{ig}}$, and the initial total energy, E_{ig} , scale identically with α and v_{im} because the ratio $E_{k,\text{ig}}/E_{\text{ig}}$ is conserved by the self-similar rescaling of the initial state.

The quality of the new scaling law obtained for hydrodynamically similar implosions (HSIs) is illustrated in Fig. 4. Once normalized to the $\alpha^{3.0} v_{\text{im}}^{-9.1}$ dependence, the scatter of the calculated points becomes remarkably lower than that in Fig. 3. The calculated values of E_{ig} follow almost perfectly the $\alpha^{3.0}$ scaling, although the power law approximation to the v_{im} dependence becomes sufficiently accurate only at $v_{\text{im}} \geq 3 \times 10^7 \text{ cm/s}$.

The newly obtained HSI scaling,

$$E_{\text{ig}} \propto \alpha^{3.0} v_{\text{im}}^{-9.1} \quad (25)$$

is quite close to the static assembled state scaling, $E_{\text{ig}} \propto \alpha^3 v_{\text{im}}^{-10}$, derived analytically in the framework of a simple isobaric model [5, 6]. From this we conclude that a significant departure of the Livermore scaling, $E_{k,\text{ig}} \propto \alpha^{1.7} v_{\text{im}}^{-5.5}$, from the $\alpha^3 v_{\text{im}}^{-10}$ law cannot be explained by the heat conduction from the hot spot and α particle self-heating, as suggested in Ref. [4], because these same processes also affect the HSI scaling. In the next section we scrutinize in more detail the role played by different physical processes in determining the scaling of E_{ig} .

4. RELATION TO THE ASSEMBLED STATE SCALING LAW

Here, we rederive and examine closely the ignition energy scaling obtained by considering assembled fuel configurations, and then discuss its relation to the Livermore and HSI scaling laws.

4.1. Static assembled state scaling

We begin with the Meyer-ter-Vehn [5] isobaric model by assuming that the DT fuel at stagnation occupies a spherical volume of radius R with a stepwise density profile,

$$\rho(r) = \begin{cases} \rho_s, & 0 \leq r \leq \xi_s R \\ \rho_c, & \xi_s R < r \leq R \end{cases} \quad (26)$$

where $\rho_s < \rho_c$, and the pressure

$$P = K\rho_s T_s = P_* \alpha \rho_c^{5/3} \quad (27)$$

is constant over the entire fuel volume $0 \leq r \leq R$. Here, ξ_s is the fractional radius of the hot spot (thermonuclear spark) and $K = 77.2 \text{ MJ}/(\text{g}\cdot\text{keV})$ is a constant. The first part of Eq. (27) is simply a definition of the spark temperature T_s under the assumption that the electron degeneracy is not important in the spark region. Having invoked the equations of mass,

$$M = \frac{4\pi}{3} R^3 [\rho_s \xi_s^3 + \rho_c (1 - \xi_s^3)] \quad (28)$$

and energy balance,

$$E = \frac{1}{2} M v_{\text{im}}^2 = \frac{3}{2} P \frac{4\pi}{3} R^3 \quad (29)$$

we readily obtain the following expression for the fuel energy

$$E = 3^5 \times 2\pi (K P_*)^3 \frac{\alpha^3 (H_s T_s)^3}{v_{\text{im}}^{10} \xi_s^3 (1 - \xi_s^3)^5} \Lambda_E \quad (30)$$

where

$$H_s = \xi_s \rho_s R \quad (31)$$

is the spark $\langle \rho r \rangle$, and

$$\Lambda_E = \left(1 - \frac{\xi_s^3 v_{\text{im}}^2}{3KT_s} \right)^5 \quad (32)$$

is a factor whose departure from 1 (less than 12% for $\xi_s = 0.55$, $v_{\text{im}} \leq 5 \times 10^7 \text{ cm/s}$ and $T_s \geq 7 \text{ keV}$) can be ignored in the parameter range of interest here. Note that, when the analysis begins with the assembled fuel state, we need a definition of the implosion velocity v_{im} , which is given by the first part of Eq. (29).

In Eq. (30) the initial fuel energy E is a function of five parameters. Being interested in the scaling of E_{ig} with the two of them (α and v_{im}), we have to determine the ignition threshold and to ‘bind’ somehow the two ‘superfluous’ degrees of freedom. One of them is removed by making the simplest realistic assumption that the ignition threshold is defined by a fixed value of the product

$$H_s T_s = \langle \rho r T \rangle_{\text{s,ig}} = \text{const.} \quad (33)$$

An obvious way to eliminate the second excessive degree of freedom is to optimize with respect to the parameter ξ_s : for given α and v_{im} , the minimum ignition energy is obtained at $\xi_s = 6^{-1/3} \approx 0.55$. Consequently, we recover the well-known scaling $E_{\text{ig}} \propto \alpha^3 v_{\text{im}}^{-10}$, which is considered as a reference case in most studies on the topic. For the discussion below, it is important to note that this static assembled state scaling corresponds to optimized (within the family of stepwise functions) ignition profiles, and that these profiles can be mapped one onto another (so long as we assume that $T_s \propto v_{\text{im}}^2$) with the similarity transformations (19)–(21) but not with the Livermore rescaling procedure (12)–(14).

4.2. Dynamic assembled state scaling

One of the most vulnerable assumptions of the static analysis is the definition (33) of the ignition threshold. Clearly, even a relatively weak dependence of $\langle \rho r T \rangle_{\text{s,ig}}$ on any of the α , v_{im} , ξ_s parameters would have a sizeable effect on the scaling of E_{ig} . In Ref. [7] it was estimated analytically (but for a different pressure profile) that $\langle \rho r T \rangle_{\text{s,ig}} \propto v_{\text{im}} \xi_s$.

Here, we have explored the dependence of the ignition threshold on the fuel parameters numerically, by performing DEIRA runs starting with the box profile assembled state as the initial condition. It was found that in all cases there was a clear optimum with respect to ξ_s at $\xi_s = 0.55$ – 0.57 . The ignition threshold $\langle \rho r T \rangle_{\text{s,ig}}$ is insensitive to α variations, but does increase with the implosion velocity (due to the reduction of the tamping effect by the cold fuel [7]), although somewhat weaker than in direct proportion to v_{im} . As a result, we obtained the following assembled state scaling law:

$$E_{\text{ig}} \propto \alpha^{3.0} v_{\text{im}}^{-7.9} \quad (34)$$

which accounts properly for the dynamic effects due to the fuel disassembly. The quality of this scaling is illustrated in Fig. 5.

Table I. Parameters of Four Marginally Igniting Fuel Configurations Simulated with the DEIRA Code in the Case of the Livermore Rescaling of the Parent Configuration

	Initial state			
v_{im} (10^7 cm/s)	3.0	3.5	4.0	5.0
M_{ig} (mg)	0.2212	0.06005	0.01962	0.00307
E_{ig} (kJ)	10.92	3.939	1.655	0.3971
$E_{\text{k,ig}}/E_{\text{ig}}$	0.912	0.934	0.948	0.966
	Stagnation			
Peak T_i (keV)	11.0	11.3	11.6	12.4
Hot spot $\langle \rho r T \rangle_{\text{s,ig}}$ ($\text{g}\cdot\text{cm}^{-2}\cdot\text{keV}$)	2.21	2.33	2.45	2.67
α_{stag} (density peak)	3.0	3.3	3.8	4.8
$E_{\text{stag}}/E_{\text{ig}}$	1.497	1.501	1.516	1.534

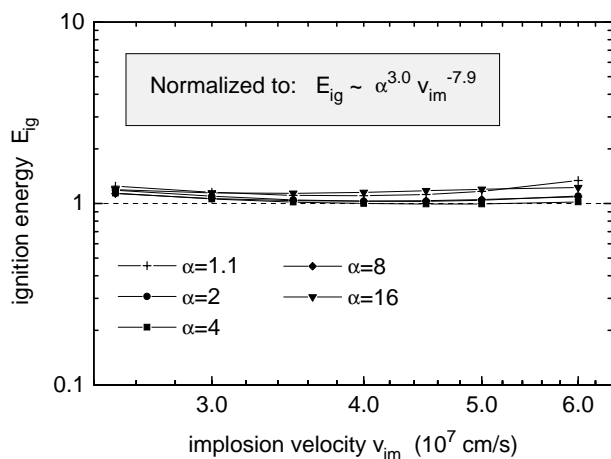


FIG. 5. Dynamic assembled state scaling: initial energy of box profile stagnation configurations, which demonstrate marginal ignition when simulated with the DEIRA code, normalized to the power law $0.9 \text{ (kJ)} \alpha^{3.0} (v_{\text{im}}/4 \times 10^7 \text{ cm/s})^{-7.9}$. The v_{im} scale is shifted to higher values as compared with Figs 2–4, because in full simulations of the implosion dynamics the stagnation energy exceeds the initial energy by about a factor of 1.5 (Table I).

With respect to the spark temperature T_s , no optimization can be performed because E_{ig} decreases monotonically with the increasing T_s . The data presented in Fig. 5 have been obtained with a fixed value of $T_s = 10$ keV, chosen on the basis of the observation that the peak ion temperature at stagnation of marginally igniting configurations, simulated with a full account of the implosion dynamics, is always close to 10–13 keV (Table I). However, within

its error bars of $a = 3.0 \pm 0.1$, $b = 8.0 \pm 0.2$, the scaling law (34) is not sensitive to whether T_s is fixed at some value above 5 keV, or is varied, for example, as $T_s = 10 \text{ keV} (v_{\text{im}}/3 \times 10^7 \text{ cm/s})^2$.

4.3. Relative role of different factors which affect the ignition energy scaling

Consider now in more detail the impact of different factors on the ignition energy scaling, beginning with the definitions of the basic physical quantities. First of all, the implosion velocity defined by Eq. (29) differs from the one which enters the Livermore and the HSI scalings. If we ignore for the moment the fact that the fuel energy at stagnation, E_{stag} , exceeds the total initial energy, $E_{\text{ig}} = E_{\text{k,ig}} + E_{\text{th,ig}}$, we conclude that the difference in v_{im} definitions is irrelevant for comparison between the HSI and the assembled state scaling laws (because the self-similar rescaling of the initial state conserves the ratio $E_{\text{k,ig}}/E_{\text{ig}}$) but should be taken into account in the case of the Livermore scaling. When the Livermore scaling for $E_{\text{k,ig}}$ is recalculated in terms of the total initial energy E_{ig} versus the redefined implosion velocity $\tilde{v}_{\text{im}} = \sqrt{2E_{\text{ig}}/M_{\text{ig}}}$, the exponent b in Eq. (1) increases to $b = 6.5 \pm 0.5$, whereas the value of $a = 1.7 \pm 0.2$ remains unaffected. Thus, different definitions of E_{ig} and v_{im} are partly (but not mainly) responsible for the difference between the Livermore scaling and the assembled state scaling. Note that the Livermore scaling for the total energy E_{ig} differs from that for its kinetic part $E_{\text{k,ig}}$ (without redefining v_{im}) by $\Delta b \approx 0.2$, $\Delta a \approx 0.05$.

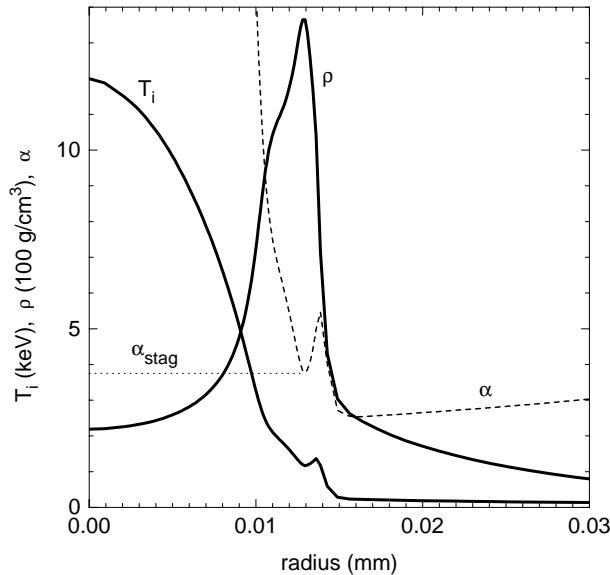


FIG. 6. Profiles of the ion temperature T_i , density ρ and entropy parameter $\alpha = P/P_*\rho^{5/3}$ at stagnation of a marginally igniting ($G_f = 8$) configuration as calculated with the initial state of Section 2.2 rescaled self-similarly to $\alpha = 2$, $v_{im} = 3.5 \times 10^7$ cm/s.

One of the main shortcomings of using the assembled state as a starting point is that the thermonuclear self-heating of the fuel prior to stagnation is not accounted for. We can readily evaluate this effect by examining how the ratio E_{stag}/E_{ig} , where E_{stag} is the total fuel energy at stagnation, changes with α and v_{im} (Table I). Our simulations indicate that the variations of E_{stag}/E_{ig} are confined to such a narrow range that the ensuing corrections to the values of exponents a and b do not exceed 0.1, independent of the rescaling procedure for the initial state. Note also that, because the ratio E_{stag}/E_{ig} has a weak tendency to increase with v_{im} , the resulting correction to the assembled state value of b should be positive, i.e. away from the Livermore scaling.

Consequently, we are led to the conclusion that the main cause for differences between differently obtained scaling laws for E_{ig} should be sought in the ignition profiles, namely in their similarity properties. A typical example of the temperature (ion), density and α parameter profiles at ignition, obtained by simulating the implosion dynamics, is shown in Fig. 6. These profiles differ significantly from the simple step functions assumed in Sections 4.1 and 4.2. The time of stagnation shown in Fig. 6 and represented in Table I is defined as the time of maximum total fuel $\langle \rho r \rangle = \int \rho dr$. Most of the fuel (about 80% by mass) outside the density peak is still imploding

with a near maximum velocity. An important feature is that the entropy parameter in the density peak, α_{stag} , exceeds considerably the initial α value in the cold fuel (Table I).

Each of the scaling laws discussed above has been established along a certain two parameter sequence of ignition profiles. Clearly, if the differences between the ignition profiles in these sequences are scale dependent, one can obtain quite different scaling laws. The dynamic assembled state scaling (34) is obtained for optimized (within the class of stepwise functions) ignition profiles, which turn out to be hydrodynamically similar to one another. The ignition profiles for the Livermore and HSI scaling laws are not optimized, at least not consistently along the corresponding sequences. The HSI scaling preserves the similarity of the hydrodynamic motion initially, when rescaling the parent configuration, although it is inevitably perturbed later due to the electron and radiative heat conduction and α particle deposition. Nevertheless, the resulting scaling law (25) is quite close to the optimized dynamic assembled state scaling (34).

For the Livermore scaling, the hydrodynamic similarity is violated twice: first in the initial conditions for the hydrodynamic motion, and then due to the dissipation processes near the time of stagnation. As a result, the Livermore scaling differs strongly from both the HSI and the assembled state scaling laws. The main cause of this difference appears to be the violation of hydrodynamic similarity in the rescaling procedure for the initial state. How such violation may result in significant scaling distortions can be illustrated in a simple manner with Eq. (30): once ξ_s is not fixed at its optimum value of 0.55 but allowed to vary with α and v_{im} , one can, evidently, observe strong departures from the $\alpha^3 v_{im}^{-10}$ scaling.

5. CONCLUSION

Our principal conclusion is that the scaling of the ignition energy E_{ig} with the peak velocity v_{im} and the entropy parameter α of imploding DT fuel, as calculated with the method employed in Ref. [4], is more sensitive to a particular subset of initial configurations, chosen to establish the scaling, than to the effects of conductive and radiative energy transport and thermonuclear self-heating in the process of hot spot formation. Since the initial states for the scaling study are formed during the preceding stage of ablative shell acceleration, the latter means that

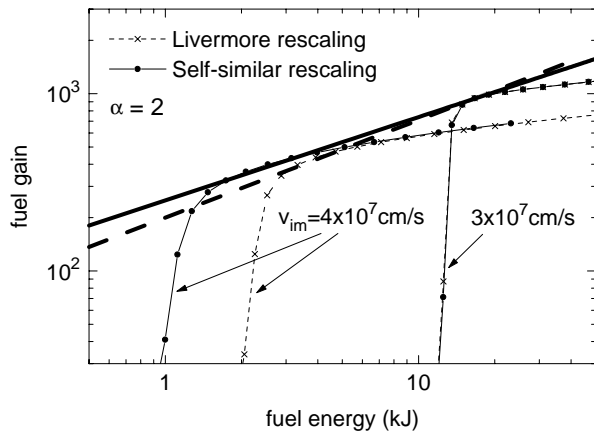


FIG. 7. Two families of gain curves calculated by applying the Livermore (13) and the self-similar (23) velocity transformations to the same initial state at $\alpha = 2$, $v_{\text{im}} = 3 \times 10^7$ cm/s. Each gain curve is obtained by performing the mass rescaling (12) of the corresponding initial state for a given value of v_{im} .

the dependence $E_{\text{ig}}(\alpha, v_{\text{im}})$ is to a large extent determined by specific constraints imposed on the drive conditions.

In particular, we find that, if the fuel pressure at peak velocity (initial state for the scaling study) varies according to the hydrodynamic similarity laws, $P \propto \alpha^{-3/2} v_{\text{im}}^5$, the ignition energy scales as $E_{\text{ig}} \propto \alpha^{3.0} v_{\text{im}}^{-9.1}$. This is contrasted with the Livermore scaling, $E_{\text{ig}} \propto \alpha^{1.7} v_{\text{im}}^{-5.5}$, which corresponds to a fixed fuel pressure at peak implosion velocity. Possible practical implications of the difference between these two scaling laws are illustrated in Fig. 7. If one starts with one and the same fusion capsule optimized for $v_{\text{im}} = 3 \times 10^7$ cm/s and then rescales it to $v_{\text{im}} = 4 \times 10^7$ cm/s, one finds that the ignition threshold obtained with the fuel pressure scaled as $P \propto v_{\text{im}}^5$ is about a factor of 2 lower than the ignition energy evaluated from the Livermore scaling.

In general, the connection between the fuel pressure P at peak velocity (initial pressure in the scaling study) and the ablative drive pressure P_a is not trivial and depends on a particular capsule drive strategy. An evident possibility to reach the hydrodynamically similar initial states of our present study is to rescale accordingly the full implosion history. Hence,

the $E_{\text{ig}} \propto \alpha^{3.0} v_{\text{im}}^{-9.1}$ scaling should apply when the peak ablation pressure is allowed to vary as $P_a \propto \alpha^{-3/2} v_{\text{im}}^5$. Although the authors of Ref. [4] have not elaborated on the relation between P and P_a , a logical assumption would be that the Livermore scaling corresponds to a significantly weaker (if any) dependence of the peak ablation pressure on α and v_{im} . The latter may be perfectly justified for the specific conditions of the NIF targets, where basic constraints on the peak drive pressure are set by the physics of laser-plasma interaction inside the hohlraum. However, in view of the high costs of potential ICF facilities, it is important to realize that under more general circumstances, when the limitations on the drive pressure are relaxed, one can obtain a significantly different dependence of the ignition threshold E_{ig} on α and v_{im} which, in particular, scales more favourably towards higher implosion velocities.

REFERENCES

- [1] LINDL, J.D., McCORRY, R.L., CAMPBELL, E.M., Phys. Today **45** (1992) 32.
- [2] LINDL, J.D., Nuovo Cimento A **106** (1993) 1467.
- [3] LINDL, J.D., Phys. Plasmas **2** (1995) 3933.
- [4] LEVEDAHL, W.K., LINDL, J.D., Nucl. Fusion **37** (1997) 165.
- [5] MEYER-TER-VEHN, J., Nucl. Fusion **22** (1982) 561.
- [6] MURAKAMI, M., MEYER-TER-VEHN, J., Nucl. Fusion **31** (1991) 1315.
- [7] BASKO, M.M., Nucl. Fusion **35** (1995) 87.
- [8] PIRIZ, A.R., Fusion Eng. Des. **32&33** (1996) 561.
- [9] BASKO, M.M., Nucl. Fusion **30** (1990) 2443.
- [10] BASKO, M.M., Teplofiz. Vys. Temp. **23** (1985) 483 [English translation: High Temp. **23** (1985) 388].

(Manuscript received 4 May 1998

Final manuscript accepted 16 September 1998)

E-mail address of M.M. Basko:

basko@drfc.cad.cea.fr or

basko@vitep5.itep.ru

Subject classification: L0, It